Selective Generation of Cu Electrodes on Ultra-Thin Glass by Femtosecond Laser Reductive Sintering of CuO

Kay Bischoff*[1], Tim Ehmes[1], Cemal Esen[2], and Ralf Hellmann[1]

[1]*Applied Laser and Photonics Group,*
University of Applied Sciences Aschaffenburg, Würzburger Str. 45, 63743 Aschaffenburg, Germany
[2]*Applied Laser Technologies,*
Ruhr University Bochum, Universitätsstraße 150, 44801 Bochum, Germany
**Corresponding author's e-mail: kay.bischoff@th-ab.de*

Copper(II)-oxide-based femtosecond reductive laser sintering is applied to selectively produce high quality and flexible copper electrodes on ultra-thin glass with thicknesses between 30 and 100 µm. To increase the precursor wettability and the later copper adhesion, the ultra-thin glass substrates are plasma activated. An amplified near infrared femtosecond laser combined with a galvanometric scanner is used to produce two-dimensional copper layers. Different laser and process parameters such as scan speed, laser power and repetition rate are varied to generate these structures with unrestricted design. The metallization rate can be significantly increased by adjusting the repetition rate in a new holistic parameter variation approach. This acceleration is accomplished by increasing the heat accumulation at higher repetition rates to reach the precursor temperature required for chemical reduction and sintering more rapidly. The copper structures are analyzed by optical microscopy, scanning electron microscopy, energy dispersive X-ray spectroscopy and 4-tip resistance measurement, respectively. In an optimized process regime, low electrical sheet resistances down to 117 mΩ/sq are achieved. A hybrid approach combining reductive laser sintering using infrared and laser drilling using ultraviolet femtosecond laser radiation is demonstrated, to produce a functional electrical circuit by employing the fundamental wavelength and the third harmonic of the same laser system.
DOI: 10.2961/jlmn.2026.01.2013

Keywords: ultra-thin glass, copper electrode, laser reductive sintering, flexible electrode, laser direct writing, laser digital patterning, femtosecond laser, ultrashort pulsed laser

1. Introduction

The interest in flexible electronics for medical, automotive, or aerospace applications has led to growing research attention on novel technologies to electrify flexible substrates [1, 2]. As the size of electronic applications decreases, the importance of substrate material increases, since it enables the realization of thinner, lighter and high-quality, durable devices. Glass substrates offer a number of advantages, including a high glass transition temperature, inertness, excellent dielectric properties and biocompatibility, which make them suitable for a wide range of applications [3, 4]. Furthermore, the thickness of borosilicate glass can be reduced to below 200 µm for the upcoming material class of ultra-thin glasses (UTG), thereby enhancing flexibility and reducing weight while maintaining stability and flatness [5]. In order to realize a variety of applications, including temperature sensors [6], bio sensors [7] and RF energy harvesting devices [8], it is necessary to electrify glass substrates through an appropriate metallization process.

A promising technology for achieving conductive metallic patterns, tracks or electrodes with no requirement for masks, vacuum, or environmentally detrimental etching processes is laser direct writing [9, 10]. Particulary reductive laser sintering uses stable copper (Cu) compounds as coated precursors in the form of salts [11], deep eutectic solvents [12], complexes [13], or oxide nanoparticles [14–17]. The laser triggers the reduction and sintering of these components to form metallic Cu. The overall process of the RLS is illustrated in Fig. 1. The use of copper(II) oxide promises high metallization velocities and low electrical resistances, and has been applied to a wide range of rigid materials, including fused silica and polymers [6, 7, 16, 18, 19]. Other research groups have also shown that flexible substrates such as PI [16, 20–23] , PET [22] or PDMS [24] can be electrified using RLS. A number of applications have already been exhibited, including heaters [16], touchscreens [22] and variety of sensor types [18, 23, 25–27].

It has been demonstrated that Cu structures with high conductivities can be manufactured using cost-effective lasers with pulse durations in the nanosecond range or continuous wave lasers [16, 20, 22, 28]. The utilization of ultrashort pulsed (USP) lasers for reductive laser sintering affords precise control over the introduced energy, thereby minimizing the heat-affected zone and consequently reducing thermal-induced damage to the substrate [15]. Moreover, the use of an USP laser enables highest quality structuring [29] or functionalization [30] of glass. Glass and above all UTG is a highly sensitive material that requires ultra-short pulsed lasers for ablative or cutting processes with high quality [29, 31, 32]. The utilization of the third harmonic of such lasers has been demonstrated to be advantageous for the processing of transparent and brittle materials [33, 34].

Prior research has illustrated the potential of hybrid USP processes for both micromachining the substrate and conducting reductive laser sintering [35]. In addition to the used CuO precursor, the process is affected by a number of laser and process parameters, including repetition rate (RR), laser power, scan speed, wavelength and spot size.

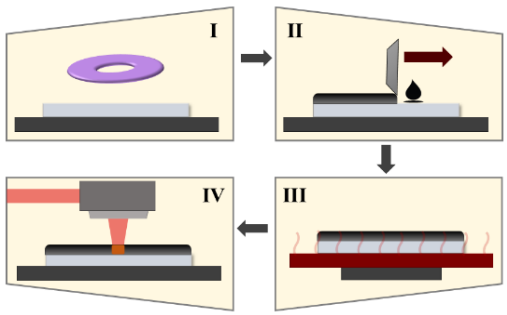

Fig. 1 The reductive laser sintering process. I: Plasma activation; II: Precursor coating; III: Drying; IV: Laser process.

In this study, we employ CuO precursor-based femtosecond reductive laser sintering for the electrification of flexible ultrathin glass, establishing a fundamental basis for the development of novel and innovative UTG-based electric devices. Furthermore, we present a systematic approach to globally compare the utilized laser parameters. The objective is to investigate the influence of the laser repetition rate and to optimize the metallization process to maximum process efficiency, quality, and conductivity by varying the power density and scan speed. Furthermore, a hybrid methodology for the integration of electrifying and ablating processes based on USP laser processes is presented.

2. Experimental

2.1 Chemicals and Materials

UTG substrates D263T eco with thicknesses of 30 and 100 µm were provided by Schott. CuO nanoparticles (40–80nm) were obtained from Iolitec. Polyvinylpyrrolidone (PVP) K12, ethylene glycol (EG) (>99%) and Ethanol (>99.8%) were purchased from Carl Roth.

2.1 Reductive Laser Sintering

The synthesis of the precursor was conducted in accordance to the methodology previously outlined by the authors [36, 37]. PVP was dissolved in EG and added to powdered CuO-NP, which was then stirred until a homogeneous viscous paste was obtained. Substance concentrations were calculated based on the mass ratios of 51:38:11 wt.% (CuO:EG:PVP). High-energy ball milling (MM 500 nano, Retsch) with a frequency of 35 Hz was employed to disperse the nanoparticles over a grinding time of 90 minutes. To reduce the viscosity and facilitate efficient grinding, ethanol was added. Following dispersion, residual ethanol was gently distilled out using a rotary evaporator (RV 3, IKA).

The RLS process is illustrated in Fig. 1. The UTG samples were plasma-activated (Zepto, Diener) in order to enhance the wetting of the UTG surface and to facilitate the formation of a homogeneous precursor layer (I). The substrates were coated by the doctor blade instrument (ZAA 3000, Proceq), generating a film thickness of approximately 10 µm (II). The coating was dried on a hot plate at 70 °C to evaporate the EG (III). A laser is employed to introduce energy selectively into the precursor, thereby facilitating the chemical reduction of the precursor to metallic Cu and its subsequent sintering to form a conductive layer (IV).

2.2 Femtosecond Laser Processing

The experiments were conducted using a multi-station laser material processing system (Optec). As illustrated in Fig. 2, the system is equipped with an USP laser (Carbide CB5, Light Conversion), which, in addition to its fundamental near infrared wavelength (IR), has a THG module for emitting ultraviolet (UV) radiation. The linear polarized laser has a maximum average power of 6 W, a minimum pulse duration of 230 fs, and a variable RR of up to 1 MHz**.** The machine features multiple beam paths, allowing for the integration of various processing stations equipped with galvanometric scanners (Scanlab Excelliscan @ IR & Raylase Miniscan @ UV) and F-theta lenses (163 mm @ IR and 56 mm @ UV) for different wavelengths. The characteristics of the system for the two wavelengths are presented in Table 1. The average laser power was determined at the sample level (Gentec), and the focus diameters were verified by means of a camera (BeamPro, Femto Easy) with pixel size 1.4 µm. While RLS was conducted at high speed with a 65 µm spot diameter in the IR wavelength, precise micromachining operations can be performed with an 11.5 µm spot in the UV.

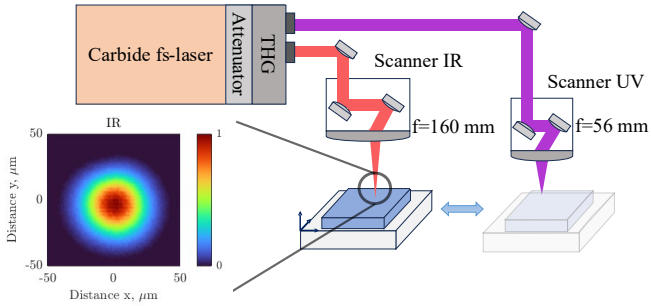

Fig. 2 Set-up for RLS in the IR with associated focus spot and micro-material processing in UV.

Table 1 Properties of the laser system in IR and UV

Parameter	Infrared	Ultraviolet	Unit
Pulse width	230		fs
Repetition rate	≤ 1000		kHz
Wavelength	1030	343	nm
Max. power	6	1.7	W
Focal diameter (1/e²)	65	11.5	µm

2.3 Evaluation Methods

An optical inspection of the produced Cu layers was conducted using a digital microscope (DMV6, Leica). High-resolution images were obtained using a scanning electron microscope (SEM) (MAIA3, Tescan). Porosity was quantified using the software ImageJ by threshold-based segmentation and calculation of the pore area fraction with the built-in measurement function. The material composition was analyzed for Cu, oxygen and carbon using the integrated energy dispersive X-ray (EDS) sensor at an acceleration voltage of 8 kV. The results were averaged from 3 regions, each measuring 300 x 300 µm. Electrical surface resistance measurements were conducted on 7 x 7 mm² Cu areas in triplicate using a four-tip measuring instrument (Loresta GX, Mitsubishi Chemical Analytech). The probe was positioned vertically and horizontally relative to the hatching direction.

3. Results and Discussion

3.1 Plasma activation of UTG surfaces

In order to provide the UTG samples with a homogeneous precursor layer and to ensure the subsequent Cu layers exhibit optimal adhesion, the wettability of the substrates was enhanced through low-pressure plasma activation and characterized using contact angle measurements. At the maximum power output of the system (100 W) and a pressure of 0.2 mbar, the activation time was varied, and the contact angle was measured with water in each case. Immediately following the activation process, the detection limit of the employed measurement method was surpassed even for short activation times. Consequently, the measurement was conducted 24 hours after activation, as illustrated in Fig. 3. An activation time of 2 min results in a notable reduction in the contact angle, exceeding half of the initial value. Contact angles were observed to decrease further with prolonged activation times. Even after the 24-hour ageing phase, a treatment time of 8 min demonstrated near-complete wetting. This behavior is consistent with documented observations on glasses [38]. For the coating of the PK, an 8 min activation and coating period was implemented immediately following coating, enabling the production of homogeneous dry layers with layer thicknesses of approximately 10 µm using the doctor blade method.

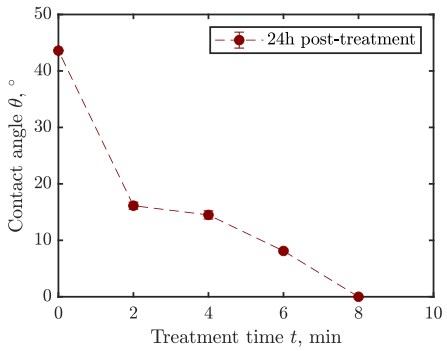

Fig. 3 Influence of the duration of plasma activation of UTG on the contact angle of water 24 h after activation.

3.1 Heat mapping for RLS parameter comparison

The impact of specific process parameters has been primarily examined under discrete conditions in the extant literature. For instance, investigations have been conducted by varying the RR of the laser while maintaining consistent values for other parameters, such as scan speed or pulse energy [16, 35]. In the field of laser material processing with pulsed laser systems, an increase in this frequency can contribute to a reduction in the inter-pulse cooling time, which may in turn influence the accumulation of heat within the processed material [39, 40]. In a mostly thermochemical process such as RLS, it is imperative to select the energy introduced and the exposure time (scan speed) with precision, given that the temperature required for reduction and sintering must be reached in the PC, and that excessive exposure time can lead to reoxidation and a deterioration in electrical conductivity [6, 19]. Should the temperature increase within the PC be affected by alterations to external factors, such as the RR, the absorption properties of the PC, or the duration of the laser pulse, the optimal point identified for a specific process condition may undergo a change.

Consequently, this study introduces a new methodology for analyzing such parameters, whereby a comprehensive range of values is examined with regard to the mean laser power and scan speed (laser spot velocity) employed for a novel process condition. A heat map of the parameter values, that classifies the quality of the RLS generates structures, can be created for an initial assessment of the influence of a particular variable. Cu surfaces with dimensions of 1 x 2 mm² are created by unidirectional hatching of individual lines with an overlap of 65% of the focus diameter, which ensures a uniform energy input [41]. This results in the formation of distinct surfaces, which are subsequently classified through optical microscopy, as illustrated in Fig. 4. At the lowest power densities, the temperature increase in the PC is insufficient to induce any change in the material. As the power density is increased further, the PC commences to undergo modification without the formation of metallic Cu becoming visible. An additional increase in temperature and/or exposure time results in the initial formation of Cu, which manifests as an inhomogeneous layer. The formation of homogeneous Cu layers is contingent upon the laser energy reaching the requisite temperature for PC reduction and the exposure time being sufficient for the reaction and sintering to occur completely. An excessive energy input will result in damage to the Cu, the precursor, or the substrate.

The heat maps for the RR of 100 kHz and 1 MHz are presented in Fig. 4. Apparently, the utilization of a RR of 1 MHz results in a considerably larger parameter window, in terms of both the usable average power density and the scan speed. This comparison suggests a strong influence of the RR and shows that comparing the same pulse energies instead of average laser power is not useful, as is otherwise common in laser material processing with pulsed lasers. Furthermore, this purely optical assessment of the Cu layers produced allows the assumption that a higher RR is associated with an acceleration of the RLS process.

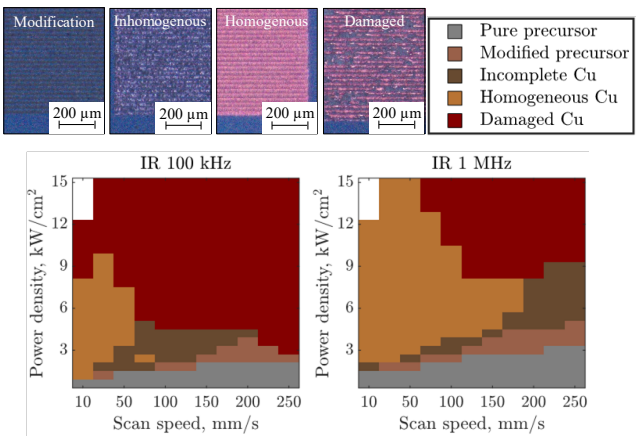

Fig. 4 Categorization and heat mapping of the emerging structures during RLS with the RR 100 kHz and 1 MHz.

3.2 Influence of the repetition rate on RLS

The impact of the RR on the morphology, elementary composition and resulting electrical resistances of the Cu layers produced was examined for RR spanning from 60 to 1000 kHz. The investigation was conducted in two stages. Initially, the ideal power densities for minimal sheet

resistance without compromising the integrity of the copper layer were ascertained (cf. Fig. 5). Subsequently, these copper surfaces were replicated under optimal conditions, and the sheet resistance was measured and evaluated in relation to the scan speed and RR (cf. Fig. 6). Variations in scan speeds and mean power densities were employed to assess the influence of these parameters on the aforementioned characteristics. For each RR, the average power density at which the lowest surface resistance is achieved was initially determined for each scan speed. As illustrated in Fig. 5, higher powers can be employed with increasing RR, a trend that is already discernible in the heat map (cf. Fig. 4). The optimal power intensities are typically the maximum that can be utilized for a given scan speed without destroying the Cu surfaces produced.

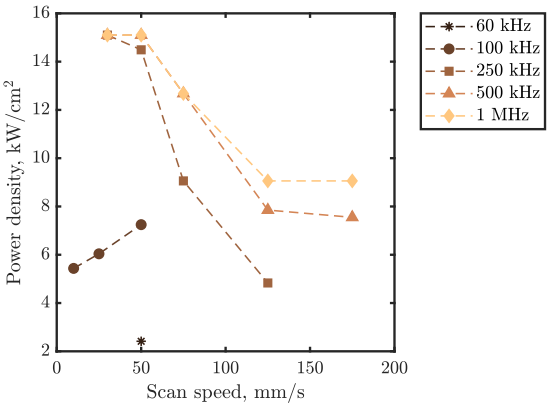

Fig. 5 Optimized power densities for the lowest surface resistances as a basis for Fig. 6.

Measurement of surface resistance:

Fig. 6 illustrates the surface resistances determined by four-tip measurements for the investigated RR, with the scan speed of the laser varied to achieve the respective optimal power densities (Fig. 5). As the objective was to create layers with the highest possible conductivity, only resistances below 1 Ω/sq are presented. The surface resistances exhibit parabolic curves, with the minimum peaks shifting towards higher scan speeds as the RR increases. For RR of 60 and 100 kHz, the highest conductivity can only be achieved at scan speeds of up to 50 mm/s. The minimum surface resistance of 962 mΩ/sq at 60 kHz is approximately double that value when 100 kHz is used. A further reduction in the minimum surface resistance, down to 117 mΩ/sq, is observed for RR above 250 kHz, although this value range is not subject to further reduction. The behavior of the resistance for high RR at scan speeds above 75 mm/s is of particular significance. While at 250 kHz, an increase in resistance to 898 mΩ/sq is observed for 125 mm/s, the resistances and errors at 500 kHz and 1 MHz increase to a significantly lesser extent of about 353 mΩ/sq. For each RR, the larger standard deviations of the measured resistances demonstrate that the processes become more unstable with increasing scan speed. The increase in these errors is shifted to higher scan speeds by selecting a high RR of 1000 kHz. The thickness of the copper layer measures about 3.5 µm.

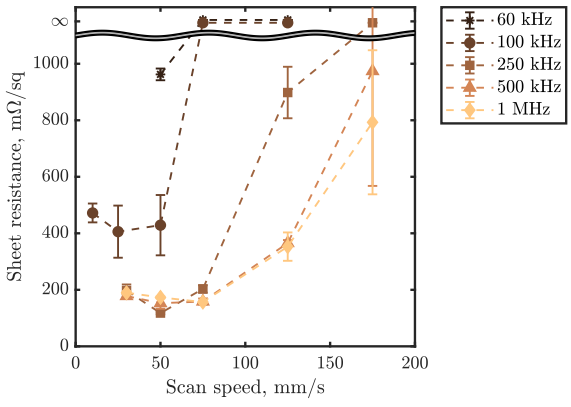

Fig. 6 Effect of scan speed on sheet resistance for RR from 60 to 1000 kHz for the evaluated power densities of Fig. 6.

Morphology of the generated Cu surfaces:

In order to gain a deeper understanding of the measured resistances for the various RR, SEM analyses were carried out on the Cu electrodes generated for 100 to 1000 kHz at a constant scan speed of 50 mm/s. The power intensities were optimized for the lowest possible resistances in each case (cf. Fig. 5). The corresponding results are presented in Fig. 7. The patterns characteristic of hatching from overlapping individual lines and the spot size employed are discernible for all RR. Cracks and porous structures are evident within the Cu layers formed. As the RR increases, the individual lines merge to a greater extent. The porosity of the Cu surfaces was quantified using image analysis, and the results are presented in Fig. 8 Evolution of porosity for RR from 100 kHz to 1 MHz in the Cu structures shown in Figure. With increasing RR, the porosity of 34.9 % at 100 kHz can be halved to 16.9 % by using 500 kHz. Furthermore, at 1 MHz, the porosity remains unaffected for the scan speed employed.

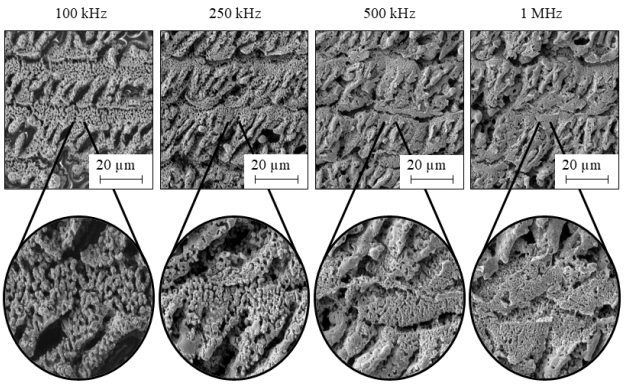

Fig. 7 SEM images of the RLS-generated Cu structures with the RR 100 kHz to 1 MHz with horizontal scan direction at 50 mm/s.

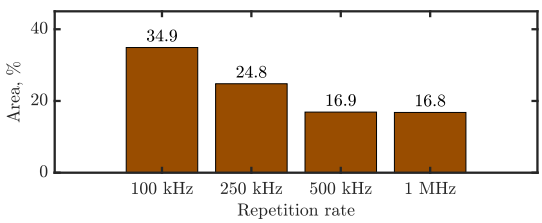

Fig. 8 Evolution of porosity for RR from 100 kHz to 1 MHz in the Cu structures shown in Figure 8.

Elemental composition:

The elemental composition of the Cu surfaces produced at varying RR and scan speeds under optimal power densities was determined through EDS analysis and visualized in Fig. 9. All electrodes were found to exhibit high concentrations of Cu, exceeding 92 %. At the lowest scan speed of 50 mm/s, the Cu generated at 250 kHz exhibited the highest atomic Cu concentration, reaching 96.6 %. The concentration of Cu decreases as the RR increases up to 250 kHz, but at higher scan speeds of 125 mm/s, a significantly greater decrease is observed. This is associated with an increase in the concentration of oxygen and carbon, which results in electrodes produced with high RR exhibiting a higher purity at higher scan speeds.

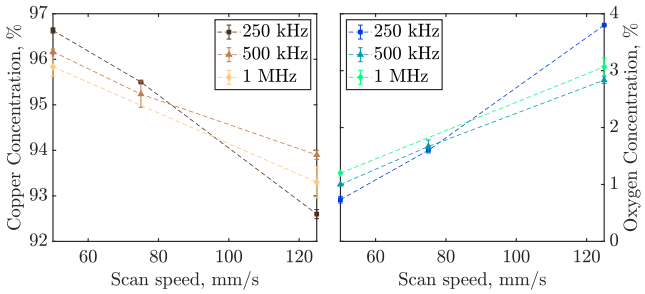

Fig. 9 EDS measurement of the elemental Cu and oxygen concentrations of the generated Cu structures with varying RR.

Discussion:

The analyses of the resulting morphologies and elemental compositions of the Cu electrodes produced at different RR and scan speeds demonstrate correlations that elucidate the observed surface resistances. The feasibility of utilizing higher power densities for higher RR can be attributed to the inverse proportionality of the pulse energy. An increase in RR at a constant power density results in a reduction in pulse fluence and an elevation in the ablation threshold of the PC to higher power densities. The copper surfaces created are unaffected by ablation, and an increased energy supply to the precursor allows for complete reduction and sintering. The application of a higher laser power to the PC enables the temperature required for reduction to be reached in a shorter exposure time, accompanied by the stronger thermal accumulation associated with higher RR. This results in two distinct effects: Firstly, the RLS process (i.e. the reduction and sintering) is already completed by the laser before the end of the exposure at low scan speeds [42]. Consequently, reoxidation can already take place at high RR, as evidenced by the elemental compositions. This results in an increased layer resistance. This effect can be offset by employing faster scanning and shorter exposure times. While the requisite exposure time for low RR is not attained at high scan speeds, the RLS process can be fully completed for high values, resulting in reduced resistance and supporting the aforementioned peak of the parabolic curves in Fig. 6. The consequence for the RLS process is that the process speed can be increased not only by employing larger focal spots (which results in a corresponding loss of resolution) [19], but also by selecting higher RR.

The impact of RR and scan speeds on layer resistances can be substantiated through SEM and EDS analyses. The porosity observed at low RR arises from the higher pulse energies associated with this setting. The incidence of each incoming laser pulse results in an abrupt heating of the PC, accompanied by the formation of gaseous decomposition products. The quantity of these gases appears to correlate with the pulse energy. The escaping gas creates voids that manifest as porous structures or induce cracking in the layer. At RR up to 500 kHz, the process occurs in smaller, more frequent bursts with lower vapor pressure, thereby reducing porosity. Furthermore, the greater accumulation of heat [40] can cause the Cu to fuse more strongly, which explains the improved homogeneity. It can be assumed that a thermal equilibrium state prevails from an RR of 500 kHz onwards and that the temperature between pulses barely fluctuates as the pulse energy decreases, so that the gases escape permanently and no longer in bursts. Consequently, there is no further decrease in porosity towards 1 MHz. Kang et al. [16] observed a comparable phenomenon with regard to crack formation. This is accompanied by a reduction in surface resistance, which is particularly evident with the rise in RR up to 250 kHz. The elevated porosity at 250 kHz in comparison to higher RR is counterbalanced by the augmented atomic Cu content. Consequently, at 250, 500 and 1000 kHz and 50 mm/s, the surface resistances are nearly identical. It consequently follows that at higher porosity, a stronger oxidation of the Cu formed can be assumed to take place, but that there is a higher reactivity for sensor applications.

The atomic concentration curves for Cu, oxygen and carbon at higher scan speeds provide evidence to support the assumption that a low RR is advantageous at low scan speeds (lower reoxidation) and that higher scan speeds require a higher RR (complete reduction at a higher temperature increase). The Cu content is observed to decrease more at low RR due to increased scan speeds, as a consequence of the reduced oxygen release and the accumulation of residual PVP in the layer.

The findings are consistent with those of Kang et al. [16], who reported the optimal resistance at a RR of 300 kHz. Roth et al. [35] achieved the highest quality at a RR of 50 kHz for a polymer substrate. However, in both studies, the pulse energy was held constant. Accordingly, the potential for increasing the power density by reducing the pulse energy and the enhanced process speed by higher RR remained uninvestigated.

Based on the measured layer thickness of the copper electrodes, the resitivity at the Cu layers with minimal sheet resistance of 117 mΩ/sq can be estimated at approximately 41 µΩ·cm. This is a multiple of the bulk resistance of pure copper, as is typical for the RLS. However, we consider the sheet resistance to be a more relevant parameter for electronic applications and summarize the work pertaining to glass in Table 2. In comparison to the surface resistances achieved with ultrashort pulsed lasers on glass, as documented with 871 mΩ/sq [42] (calculated on the basis of the given resistivity and layer thickness), the values achieved in the present work demonstrate a significant improvement. The resulting resistance was considerably lower, which ensured a higher quality of the generated Cu as well as a superior sintering process and, additionally, a multiplication of the process speed. In comparison to the values achieved with nanosecond or continuous wave lasers in the range of 30 mΩ/sq [16, 20] for generated Cu lines, the resistance values are increased. However, these lasers do not provide the

potential for additional qualitative material processing in a hybrid process. Moreover, it can be postulated that the overlapping regions that emerge when individual lines are hatched may result in a reduction in the overall resistance of the surface. The findings of this study demonstrate that the creation of highly conductive structures can be achieved at an increased process speed through the utilization of an elevated scan speed. This improvement in time efficiency was primarily achieved by increasing the RR.

Table 2 Comparison of the surface resistances achieved on glass using CuO-based RLS (* calculated from the specified resistivity and layer thickness)

Author	Pulse duration	Scan speed, (mm/s)	Surface Resistance, (mΩ/sq)
Mizoshiri et al. [42]	fs	5	871*
Arakane et al. [15]	fs	1	66,000*
Kang et al. [16]	ns	30	31*
Back et al. [20]	ns	30	30*
This work	fs	50 125	117 353

3.3 Applications

Generation of complex Cu electrode designs:

Utilizing the ideal conditions found for the efficient generation of high quality, precise and conductive Cu layers, complex geometries were created by hatching on the 30 µm UTG at a RR of 1 MHz, a scan speed of 75 mm/s and a power density of 12.7 kW/cm². Fig. 10 (top) demonstrates the high resolution, precision and homogeneity of such conductors in the form of a functional heating meander especially in the peripheral areas, which can be applied by current to heat up the UTG to up to 100 °C. In addition to geometry changes (conductor width and number of windings), and by adjusting the laser and process parameters to slower scan speeds (cf. Fig. 6), this process enables the degree of reoxidation in the copper produced to be adjusted, and thus the resistance and heating power of the structure [43].

As illustrated in Fig. 10 (bottom), the fabrication of a complex electrode in the form of the Aschaffenburg castle has been achieved, thereby demonstrating the highest degree of design freedom. Modifications can be effortlessly executed by adjusting the CAD file. As demonstrated in our previous investigations [19], the resolution of the CuO-based RLS is dependent on the focus diameter employed. Here, high-quality single lines with widths in the range of the focal diameter are achieved, as depicted in the inset of Fig. 10. The selection of an f-Teta objective with a reduced focal length has facilitated the attainment of line widths less than 20 µm through the utilization of fast galvanometer scanners [16]. It has been demonstrated that ultra-fine focus spots of 1.3 µm can produce line widths of 5-10 µm when employing microscope objectives [43].

Furthermore, the mechanical flexibility of the resulting Cu layer is evaluated by means of substrate bending, and no delamination of the layer is observed thus demonstrating the potential for this direct writing technology to be used for future UTG-based flexible devices.

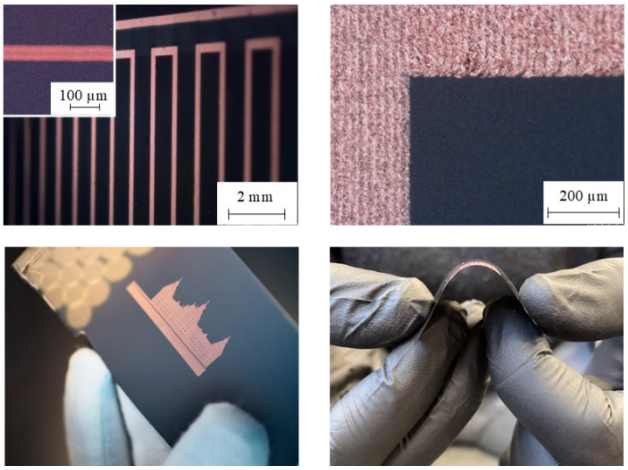

Fig. 10 Demonstration of the geometric freedom, quality and flexibility of Cu structures fabricated on 30µm UTG.

Hybrid laser processing:

The hybrid laser process is demonstrated on the multifunctional laser system by inserting an LED through the UTG and establishing contact with the conductor tracks generated by RLS. The initial stage of the process involves the creation of the conductor paths and contact pads at the IR station. Subsequently, at the UV station, holes with a diameter of 600 µm for the contact plugs are drilled by remote cutting. For this purpose, the entire contour was scanned multiple times at a scan speed of 300 mm/s and a RR of 100 kHz. As illustrated in Fig. 11, the resulting Cu layer remains almost completely intact, and the UTG shows no chipping. Despite the fact that the actual copper production using RLS could also be achieved by employing longer pulsed lasers [16, 20, 22, 28], the ultrashort pulsed laser utilized for RLS, as well as for drilling and cutting the UTG with the highest quality, demonstrates the potential to produce several processing steps in the manufacturing of complex devices with just one tool in a hybrid approach. An additional advantage of the USP cutting process is that, due to the low heat input, there is no visible discolouration of the copper indicating reoxidation near the cut edge. In the next step, the LED is inserted through the aforementioned holes and electrically contacted using a silver conductive paste. Upon the application of a voltage, the LED function is demonstrated.

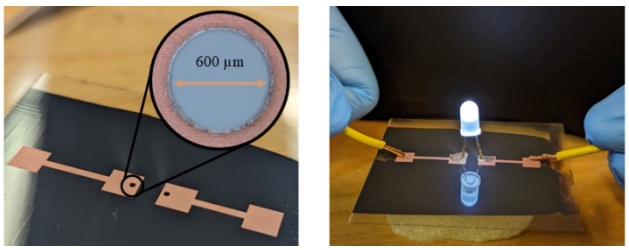

Fig. 11 Demonstration of the functionality of RLS produced traces combined with UV laser cut holes as a hybrid femtosecond laser-based manufacturing approach.

4. Conclusion

In this study, ultrathin glass was electrified for the first time using a vacuum-free, maskless and flexible process, the reductive laser sintering, to produce conductive Cu tracks and electrodes. The most significant findings are as follows:

- The adaptation of the plasma activation of UTG ensures good wetting and the formation of homogeneous dry layers of the CuO precursor with good adhesion
- Heat mapping can be employed to facilitate efficient identification of influencing factors in RLS
- In contrast to the preceding studies, which varied only one parameter, this study analyzed resistance across a wide range of scan speed and laser power combinations, thereby identifying the optimal settings for each RR
- Surface resistance down to 117 mΩ/sq and a resistivity of about 41 μΩ·cm are achieved at high scan speeds
- High-resolution electrode designs, heating structures and hybrid USP processes were demonstrated on UTG

The findings of this research provide a foundation for the utilization of ultra-thin glass through reductive laser sintering and hybrid USP laser processes in a multitude of other flexible applications.

Acknowledgments

We gratefully acknowledge funding by German Federal Ministry of Education and Research project EFP-LOC (grant number FKZ 13FH153KX0) and project ZDF-Laser (grant number13FH087IN0). We thank Schott for providing the UTG samples.

References

[1] K. J. Yu, Z. Yan, M. Han, and J. A. Rogers: npj Flex. Electron., 1, (2017) 4.
[2] D. Corzo, G. Tostado-Blázquez, and D. Baran: Front. Electron., 1, (2020) 594003.
[3] S. Garner, S. Glaesemann, and X. Li: Appl. Phys. A, 116, (2014) 403.
[4] S. M. Garner and H. Huang: "Flexible Glass", ed. by S. M. Garner, (Wiley, Weinheim, 2017) p. 1.
[5] G. C. Righini, J. Krzak, A. Lukowiak, G. Macrelli, S. Varas, and M. Ferrari: Opt. Mater., 115, (2021) 111011.
[6] M. Mizoshiri, S. Arakane, J. Sakurai, and S. Hata: Appl. Phys. Express, 9, (2016) 36701.
[7] I. I. Tumkin, E. M. Khairullina, M. S. Panov, K. Yoshidomi, and M. Mizoshiri: Materials, 14, (2021) 2493.
[8] J. Yunas, N. H. Mohd Yunus, J. Sampe, and A. B. Nandiyanto: 2020 IEEE International Conference on Power and Energy (PECon), Penang, Malaysia, (2020) 362.
[9] A. A. Manshina, I. I. Tumkin, E. M. Khairullina, M. Mizoshiri, A. Ostendorf, S. A. Kulinich, S. Makarov, A. A. Kuchmizhak, and E. L. Gurevich: Adv. Funct. Mater., 34, (2024) 2401864.
[10] T. Pinheiro, M. Morais, S. Silvestre, E. Carlos, J. Coelho, H. V. Almeida, P. Barquinha, E. Fortunato, and R. Martins: Adv. Mater., 36(29), (2024) e2402014.
[11] J. Jones, M. R. Snowdon, S. Rathod, and P. Peng: Flex. Print. Electron., 8, (2023) 15008.
[12] E. Khairullina, A. Shishov, D. Gordeychuk, L. Logunov, A. Levshakova, V. B. Sosnovsky, A. Koroleva, V. Mikhailovsky, E. L. Gurevich, I. Chernyshov, M. S. Panov, and I. Tumkin: J. Mater. Sci., 58, (2023) 9322.
[13] M. Mizoshiri, K. Aoyama, A. Uetsuki, and T. Ohishi: Micromachines, 10, (2019) 401.
[14] M. Mizoshiri, T. D. Tran, and K. V. T. Nguyen: Nanomaterials, 14, (2024) 1584.
[15] S. Arakane, M. Mizoshiri, and S. Hata: Jpn. J. Appl. Phys., 54, (2015) 06FP07.
[16] B. Kang, S. Han, J. Kim, S. Ko, and M. Yang: J. Phys. Chem. C, 115, (2011) 23664.
[17] V. B. Nam, T. T. Giang, S. Koo, J. Rho, and D. Lee: Nano Converg., 7, (2020) 23.
[18] S. Kefer, K. Bischoff, G.-L. Roth, J. Haubner, B. Schmauss, and R. Hellmann: Adv. Opt. Mater., 9, (2021) 2002203.
[19] K. Bischoff, C. Esen, and R. Hellmann: Procedia CIRP, 124, (2024) 629.
[20] S. Back and B. Kang: Opt. Lasers Eng., 101, (2018) 78.
[21] Y. Huang, X. Xie, M. Li, M. Xu, and J. Long: Opt. Express, 29, (2021) 4453.
[22] V. Binh Nam, T. Thi Giang, and D. Lee: Appl. Surf. Sci., 570, (2021) 151179.
[23] J. Zhao, Z. Yu, Z. Tu, and H. Bian: Micromachines, 13, (2022) 1103.
[24] M. Mizoshiri, Y. Ito, J. Sakurai, and S. Hata: Proc. SPIE, 10167, (2017) 101671G.
[25] J. Cheng, X. Liu, W. Kong, Q. Lei, Z. Yu, and D. Liu: Phys. Status Solidi A, 221, (2024) 2300334.
[26] S. Arakane, M. Mizoshiri, J. Sakurai, and S. Hata: J. Micromech. Microeng., 27, (2017) 055013.
[27] M. Mizoshiri, K. Nishitani, and S. Hata: Micromachines, 9, (2018) 165.
[28] M. K. Rahman, Z. Lu, and K.-S. Kwon: AIP Adv., 8(9), (2018) 95008.
[29] S. Schwarz, S. Rung, C. Esen, and R. Hellmann: Opt Express, 26, (2018) 23287.
[30] K. Bischoff, P. Quigley, A. Hohnholz, P. Jäschke, and S. Kaierle: Procedia CIRP, 94, (2020) 924.
[31] K. L. Wlodarczyk, A. Brunton, P. Rumsby, and D. P. Hand: Opt. Lasers Eng., 78, (2016) 64.
[32] H. Shin, J. Noh, and D. Kim: Opt. Laser Technol., 138, (2021) 106921.
[33] Y. Yang, K. Bischoff, D. Mücke, C. Esen, and R. Hellmann: J. Laser Appl., 36, (2024) 012001.
[34] K. Bischoff, D. Mücke, G.-L. Roth, C. Esen, and R. Hellmann: Polymers, 14, (2022) 3065.
[35] G.-L. Roth, J. Haubner, S. Kefer, C. Esen, and R. Hellmann: Opt. Lasers Eng., 137, (2021) 106362.
[36] K. Bischoff, C. Esen, and R. Hellmann: Nanomaterials, 13, (2023) 2693.
[37] K. Bischoff, D. Mücke, A. Schubert, C. Esen, and R. Hellmann: Liquids, 4, (2024) 382.
[38] T. Dey and D. Naughton: J. Sol-Gel Sci. Technol., 77, (2016) 1.

[39] S. Juodkazis, H. Misawa, and I. Maksimov: Appl. Phys. Lett., 85, (2004) 5239.
[40] R. Weber, T. Graf, P. Berger, V. Onuseit, M. Wiedenmann, C. Freitag, and A. Feuer: Opt Express, 22, (2014) 11312.
[41] S. Schwarz, S. Rung, C. Esen, and R. Hellmann: J. Laser Micro Nanoeng., 13, (2018) 292.
[42] Mizue Mizoshiri, Shun Arakane, Junpei Sakurai, and Seiichi Hata, M. Mizoshiri, S. Arakane, J. Sakurai, and S. Hata: Int. J. Autom. Technol., 10, (2016) 934.
[43] M. Mizoshiri, Y. Ito, S. Arakane, J. Sakurai, and S. Hata: Jpn. J. Appl. Phys., 55, (2016) 06GP05.

(Received: September 1, 2025, Accepted: December 7, 2025)